

# Influence of atomic radiative and collisional processes on the plasma modeling of $\text{Mg}^{10+}$ at low electron densities

D. M. Mitnik and M. S. Pindzola

*Department of Physics, Auburn University, Auburn, Alabama 36849*

D. C. Griffin

*Department of Physics, Rollins College, Winter Park, Florida 32789*

(Received 7 March 2000; revised manuscript received 7 July 2000; published 9 November 2000)

In this paper, we report on theoretical calculations of electron-impact excitation cross sections and radiative transition rates for  $\text{Mg}^{10+}$ . The excitation cross sections were calculated using semirelativistic close-coupling and fully relativistic distorted-wave theory and the radiative rates were determined using semirelativistic and fully relativistic atomic-structure theory. After the solution of the corresponding collisional-radiative equations, the  $K\alpha_2/K\alpha_1$  ( $1s2p\ ^3P_1 \rightarrow 1s^2\ ^1S_0$  over  $1s2p\ ^1P_1 \rightarrow 1s^2\ ^1S_0$ ) emission line ratio and the  $K\beta_2/K\beta_1$  ( $1s3p\ ^3P_1 \rightarrow 1s^2\ ^1S_0$  over  $1s3p\ ^1P_1 \rightarrow 1s^2\ ^1S_0$ ) emission line ratio were calculated as a function of electron temperature and density. The various scattering calculations involving different numbers of levels enabled us to study the influence of resonance structures and cascades from highly excited levels on the collisional-radiative modeling and we found that they have little effect on the level populations. However, even in this ten-times ionized species, the effects of orbital relaxation are found to be important in the determination of accurate electric-dipole radiative transition rates. Both line ratios were found to be strongly affected by whether the magnetic-dipole radiative transition from the  $1s2s\ ^3S_1$  level to the ground state was included or not. At very low electron densities, the  $1s2s\ ^1S_0$  two-photon transition to the ground state also has an effect on the  $K\alpha_2/K\alpha_1$  line ratio. In addition, we found that the line ratios are enhanced at high temperatures by radiative and dielectronic recombination from the hydrogenic  $\text{Mg}^{11+}$  ion. However, the dielectronic satellite lines have no effect on the line ratios for the low-density astrophysical, solar, and magnetic-fusion plasmas considered in this paper.

PACS number(s): 34.80.Kw, 52.20.Fs

## I. INTRODUCTION

Spectral line emission from atomic ions of the helium isoelectronic sequence may be used as a temperature and density diagnostic for a variety of laboratory and astrophysical plasmas. An important population mechanism for the excited states of radiating atomic ions is electron-impact excitation from ground and metastable states. In the present investigation, we have applied semirelativistic close-coupling [1] and fully relativistic distorted-wave [2] scattering theory to the calculation of electron-impact excitation cross sections of  $\text{Mg}^{10+}$ . The most complete  $R$ -matrix close-coupling calculations [3] to date for  $\text{Mg}^{10+}$  included only 11  $LS$  terms and did not determine the excitation cross sections between fine-structure levels. The results of two  $R$ -matrix calculations are reported below, one involving 11  $LS$  terms of the six configurations:  $1s^2$ ,  $1s2l$ , and  $1s3l$ , and a second involving 19  $LS$  terms of the ten configurations:  $1s^2$ ,  $1s2l$ ,  $1s3l$ , and  $1s4l$ . Using a recently developed intermediate-coupling frame transformation [4] of the  $R$ -matrix  $K$  matrices calculated in  $LS$  coupling, cross sections have been determined for all the transitions among the 17  $LSJ$  levels of the first calculation and the 31  $LSJ$  levels of the second calculation. We have also carried out fully relativistic distorted-wave calculations for the excitations between the 31 levels of the configurations:  $1s^2$ ,  $1s2l$ ,  $1s3l$ , and  $1s4l$ .

Using the collisional rate coefficients, supplemented by

further semirelativistic and fully relativistic atomic structure calculations for the radiative rates among the  $LSJ$  levels, we have applied collisional-radiative theory [5] to calculate level populations and line emissivities for  $\text{Mg}^{10+}$  as a function of electron temperature and density. In particular, we have examined the  $K\alpha$  line ratio involving the  $K\alpha_2$  ( $1s2p\ ^3P_1 \rightarrow 1s^2\ ^1S_0$ ) and  $K\alpha_1$  ( $1s2p\ ^1P_1 \rightarrow 1s^2\ ^1S_0$ ) transitions and the  $K\beta$  line ratio involving the  $K\beta_2$  ( $1s3p\ ^3P_1 \rightarrow 1s^2\ ^1S_0$ ) and  $K\beta_1$  ( $1s3p\ ^1P_1 \rightarrow 1s^2\ ^1S_0$ ) transitions. Both line ratios provide a very useful electron-temperature diagnostic for heliumlike plasmas. The heliumlike  $K\alpha$  emission has been studied in detail in tokamaks [6], and those studies demonstrated the great utility of the  $K\alpha$  spectra for determining the plasma electron temperature, the ion transport coefficients, the fraction of non-Maxwellian electrons, the toroidal plasma rotation velocity, and the plasma ion temperatures. The  $K\beta$  spectra are important spectral diagnostics of laser-produced plasmas in inertial confinement fusion research [7]. In addition, the utility of  $K\beta$  spectra as a diagnostic of the electron temperature for tokamaks has been recently illustrated [8,9].

In this paper, we have investigated the influence of different atomic processes on the plasma modeling of  $\text{Mg}^{10+}$  ions at low electron densities. We have compared the results obtained by doing different calculations for the excitation cross sections and the radiative transitions. In particular, we have studied the influence of resonance structures on the excitation cross sections; the effect of the highly excited levels on

the population of the low-lying levels; and relativistic, orbital-relaxation, and term-dependent effects on the electric-dipole radiative rates. We have also investigated the contribution to the line intensity from radiative and dielectronic recombination of the hydrogenic  $\text{Mg}^{11+}$  ion and the effects of overlapping dielectronic satellite transitions.

Our focus on these two emission line ratios also provides support for ongoing spectral measurements of highly charged atomic ions under well-controlled laboratory conditions using an electron-beam ion trap [10]. In particular, experimental results for the  $K\beta$  line ratios on both tokamaks and ion traps, are consistently higher than the predicted theoretical values [8,11], and detailed studies are required in order to identify the factors that contribute to these discrepancies. It is essential for any further refinement of the collisional-radiative modeling to have an accurate atomic data base, and this has also been provided in this paper. The remainder of this paper is organized as follows: in Sec. II we present our atomic-scattering and radiative transition rate calculations, in Sec. III we present our line emission ratio calculations, and in Sec. IV we summarize our findings.

## II. ATOMIC STRUCTURE AND RATE CALCULATIONS

### A. Atomic scattering calculations

Our application of  $R$ -matrix theory to the calculation of electron-impact excitation cross sections and rate coefficients is based on the RMATRIX I atomic-scattering package [12]. The bound-state radial orbitals for  $\text{Mg}^{10+}$  were calculated using Froese-Fischer's Hartree-Fock program [13]. The  $1s$  orbital was generated from a Hartree-Fock calculation of the  $1s^2$  ground configuration, while the remaining  $nl$  orbitals ( $n=2,3,4$ ;  $l=0$  to  $n-1$ ) were generated from frozen-core configuration-average Hartree-Fock (CAHF) calculations for the  $1s nl$  excited configurations. In order to compare our cross sections with the previous 11-state  $R$ -matrix calculation [3], we first performed two calculations in  $LS$  coupling: one included the 11  $LS$  terms belonging to the six configurations  $1s^2$ ,  $1s2l$ , and  $1s3l$ , while a second calculation involved 19  $LS$  terms of the ten configurations  $1s^2$ ,  $1s2l$ ,  $1s3l$ , and  $1s4l$ . The size of the  $R$ -matrix box was equal to 4.25 a.u. for the 11- $LS$ -state calculation and 6.62 a.u. for the 19- $LS$ -state calculation. To obtain a good representation of the continuum up to a maximum energy of 300 Ryd, 35 and 50 continuum basis orbitals per angular momentum were used for the 11- $LS$ -state and 19- $LS$ -state calculations, respectively. We included all  $LS\Pi$  partial waves up to  $L=14$ ; this was sufficiently complete for comparison of cross sections from the ground state.

The level of agreement between our two  $LS$  calculations with each other and with the 11-state calculation of Tayal [3] is illustrated in Figs. 1 and 2. In Fig. 1, we show the electron-impact excitation cross section from the  $1s^2 \ ^1S$  ground term to the  $1s2p \ ^3P$  excited term. In the upper part of Fig. 1, the results of the present 11- $LS$  state calculation are shown, in comparison to the results of Tayal [3]. In the lower part of Fig. 1, the cross section from the 19- $LS$  state calculation is shown. Apart from the strength of some very narrow reso-

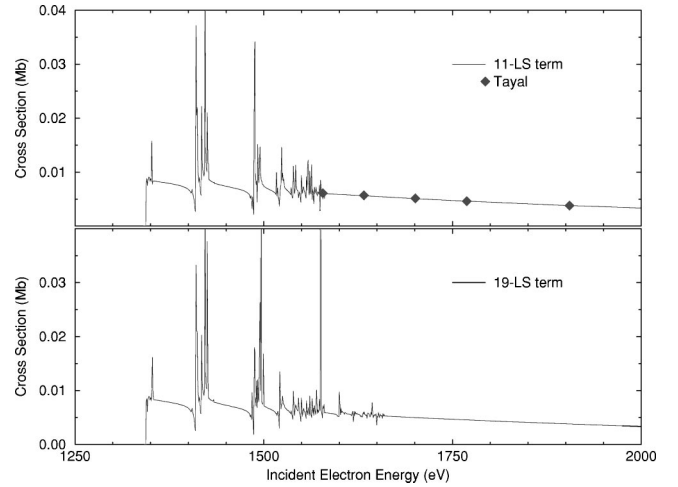


FIG. 1. Electron-impact excitation cross section for the  $1s^2 \ ^1S \rightarrow 1s2p \ ^3P$  transition in  $\text{Mg}^{10+}$ . Upper part: 11- $LS$  state  $R$ -matrix calculation. The diamonds are results from Ref. [2]. Lower part: 19- $LS$  state  $R$ -matrix calculation.

nances and the small structure corresponding to resonances attached to terms of the  $1s4l$  configurations, the agreement between the 11-state and 19-state calculations is excellent, and they both are in good agreement with the results of Tayal [3]. In Fig. 2, we show the cross sections for the  $1s^2 \ ^1S \rightarrow 1s2p \ ^1P$  transition. We also find very good agreement between the present 11-state and 19-state calculations and the results of Tayal [3] for this transition.

In order to generate level-to-level effective collision strengths for collisional-radiative modeling in this ion, we performed intermediate-coupling  $R$ -matrix calculations using the intermediate-coupling frame transformation (ICFT) method [4]. By employing multichannel quantum-defect theory, unphysical  $K$  matrices were first generated on a relatively coarse energy mesh from our  $R$ -matrix calculations in pure  $LS$  coupling. Next, these unphysical  $K$  matrices were

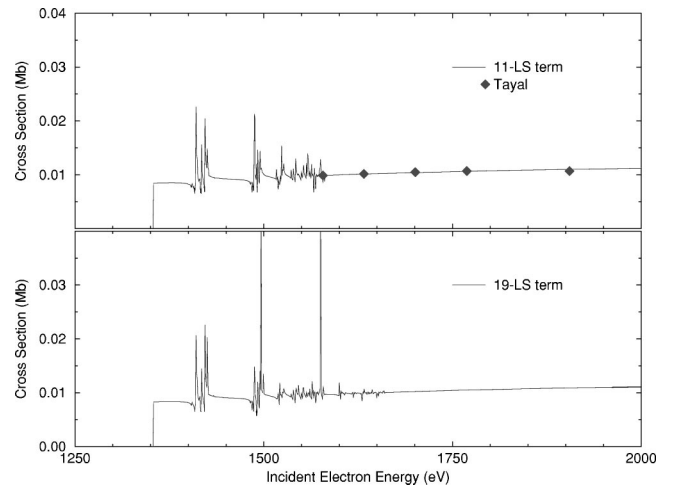


FIG. 2. Electron-impact excitation cross section for the  $1s^2 \ ^1S \rightarrow 1s2p \ ^1P$  transition in  $\text{Mg}^{10+}$ . Upper part: 11- $LS$  state  $R$ -matrix calculation. The diamonds are results from Ref. [2]. Lower part: 19- $LS$  state  $R$ -matrix calculation.

transformed algebraically to pure  $jK$  coupling, and then transformed to full intermediate coupling via term-coupling coefficients. These unphysical  $K$  matrices vary smoothly with energy and can be interpolated onto a fine energy mesh in order to later resolve narrow resonance structures. In this case, we used 5000 mesh points in the energy region of the excitation thresholds. Finally, using multichannel quantum-defect theory, we generated the physical  $K$  matrices from the unphysical ones. This ICFT method has been shown to yield cross sections, including the detailed resonance structure, in excellent agreement with full Breit-Pauli  $R$ -matrix calculations [4].

However, the unphysical  $K$  matrices for  $LS\Pi$  partial waves from  $L=0$  to 14 only allowed us to generate intermediate-coupled physical  $K$  matrices for  $J\Pi$  partial waves from  $J=0$  to 12.5. A partial-wave sum over this set of  $K$  matrices is not sufficiently complete to generate effective collision strengths for collisional-radiative modeling calculations over a wide range of temperatures. Thus, we also performed no-exchange  $LS$   $R$ -matrix calculations for all  $LS\Pi$  partial waves from  $L=12$  to 60. We then used the ICFT method to generate intermediate-coupling  $K$  matrices for all  $J\Pi$  partial waves from  $J=13.5$  to  $J=58.5$ . These high- $J$  contributions were then topped up for the dipole-allowed transitions using a method originally described by Burgess [14] and implemented in our ICFT program for intermediate coupling. Additionally, the nondipole transitions were topped up assuming a geometric series in  $J$ . These ICFT calculations allowed us to determine intermediate-coupling cross sections and effective collision strengths between the 17 levels arising from the 11 terms included in the 11-state  $LS$  calculation and between the 31 levels arising from the 19 terms included in the 19-state  $LS$  calculation.

As a completely independent test of our ICFT results, we applied relativistic distorted-wave theory to the calculation of excitation cross sections using the HULLAC atomic-scattering package [15]. In this package, the atomic structure is calculated by using Klapisch *et al.*'s fully relativistic RELAC program [16]. The main idea of this approach is the introduction of an analytic central potential whose screening parameters are determined by minimizing the first-order relativistic energy of a set of configurations. The collisional excitation cross sections are calculated in the distorted-wave approximation. This package uses the factorization-interpolation method [2], which significantly improves the computational efficiency for the calculation of the radial integrals.

In Fig. 3, we show the electron-impact excitation cross sections for the  $1s^2\ ^1S_0 \rightarrow 1s2p\ ^3P_1$  and  $1s^2\ ^1S_0 \rightarrow 1s2p\ ^1P_1$  transitions in the upper and lower parts, respectively. Both the 31-state ICFT  $R$ -matrix and relativistic distorted-wave results are presented. The results of the two calculations are in very good agreement, apart from the fact that we have not included resonance contributions in the distorted-wave calculations. In the upper part of Fig. 4, we show the excitation cross sections for the  $1s^2\ ^1S_0 \rightarrow 1s3p\ ^3P_1$  transition. The agreement in the background excitation cross sections between the two calculations is also very good. The excitation cross sections for the  $1s^2\ ^1S_0$

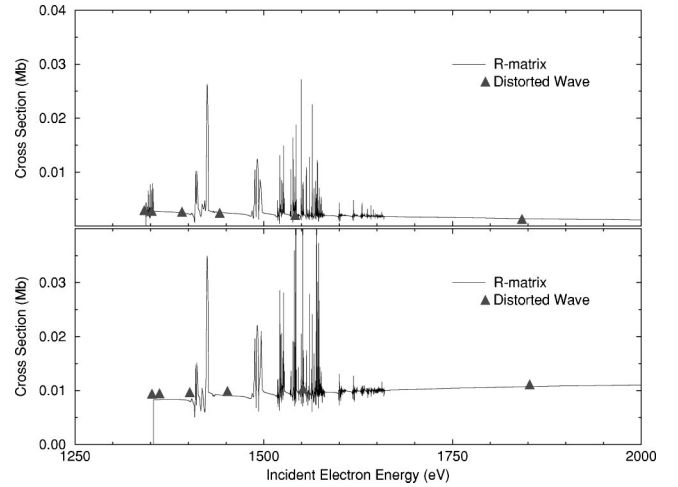


FIG. 3. Electron-impact excitation cross section for the  $1s^2 \rightarrow 1s2p$  transitions in  $\text{Mg}^{10+}$ . Upper part: transition to the  $1s2p\ ^3P_1$  level. Solid curve: 19- $LS/31$ - $LSJ$  state  $R$ -matrix calculation. Triangles: relativistic distorted-wave calculation. Lower part: transition to the  $1s2p\ ^1P_1$  level. Solid curve: 19- $LS/31$ - $LSJ$  state  $R$ -matrix calculation. Triangles: relativistic distorted-wave calculation.

$\rightarrow 1s3p\ ^1P_1$  transition is shown in the lower part of this figure. The small discrepancy between the background cross sections is most likely due to the coupling effects included in the  $R$ -matrix calculation. We conclude that, for  $\text{Mg}^{10+}$ , the relativistic effects do not have a predominant role in the calculation of the background cross sections, and they can be accounted for very well by using a Breit-Pauli approximation.

## B. Radiative rate calculations

To carry out collisional-radiative modeling for  $\text{Mg}^{10+}$ , we need both collisional excitation rates and radiative decay

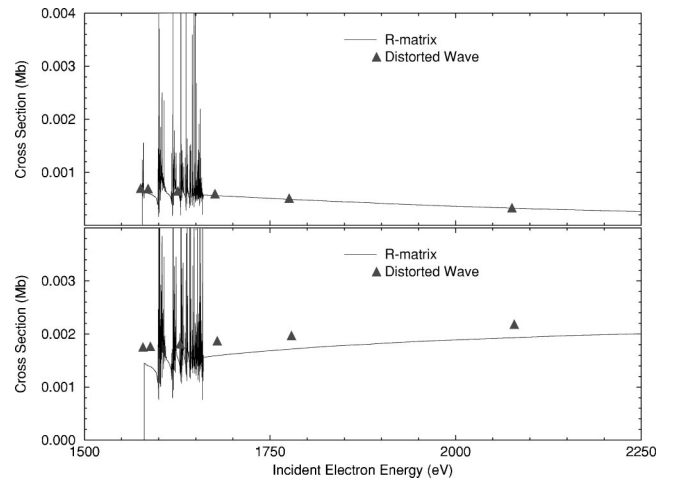


FIG. 4. Electron-impact excitation cross section for the  $1s^2 \rightarrow 1s3p$  transitions in  $\text{Mg}^{10+}$ . Upper part: transition to the  $1s3p\ ^3P_1$  level. Solid curve: 19- $LS/31$ - $LSJ$  state  $R$ -matrix calculation. Triangles: relativistic distorted-wave calculation. Lower part: transition to the  $1s3p\ ^1P_1$  level. Solid curve: 19- $LS/31$ - $LSJ$  state  $R$ -matrix calculation. Triangles: relativistic distorted-wave calculation.

TABLE I. Energies ( $E$ ) and electric dipole radiative rates ( $A$ ) for  $\text{Mg}^{10+}$ , from a fully relativistic parametric potential calculation (HULLAC) calculation, a Breit-Pauli configuration-interaction calculation using configuration-average Hartree-Fock orbitals (CAHF), and a Breit-Pauli configuration-interaction calculation using orbitals generated from a multi-configuration Hartree-Fock calculation that includes orbital relaxation and term dependence (MCHF).

Transition	HULLAC		CAHF		MCHF	
	$E$ (eV)	$A$ (Hz)	$E$ (eV)	$A$ (Hz)	$E$ (eV)	$A$ (Hz)
$K\alpha_2$	1342.77	$1.92 \times 10^{10}$	1343.92	$2.63 \times 10^{10}$	1342.49	$3.21 \times 10^{10}$
$K\alpha_1$	1352.92	$2.10 \times 10^{13}$	1353.96	$2.01 \times 10^{13}$	1351.92	$1.97 \times 10^{13}$
$K\beta_2$	1577.07	$5.65 \times 10^9$	1577.92	$8.29 \times 10^9$	1576.19	$1.01 \times 10^{10}$
$K\beta_1$	1580.12	$6.81 \times 10^{12}$	1580.66	$5.73 \times 10^{12}$	1578.78	$5.45 \times 10^{12}$

rates. For this purpose, we calculated all electric-dipole radiative rates between the levels. The dominant radiative transition rates to the ground level are shown in Table I, obtained using both the HULLAC code and a Breit-Pauli configuration-interaction calculation using CAHF radial orbitals. Unlike the excitation processes, these results show a noticeable discrepancy in the rates for the transitions from the  $^3P_1$  levels. One might expect these differences to have an effect on line emissivity calculations, thus they need to be determined as accurately as possible. Selecting a method for an accurate calculation of the intercombination transitions is a delicate issue, due to the competition between term dependence and relativistic effects.

$\text{Mg}^{10+}$  is a borderline case that demands a careful analysis to decide whether a relativistic or nonrelativistic method has to be employed. In a systematic study of the  $1s2p\ ^3P_1 - 1s^2\ ^1S_0$  and  $1s3p\ ^3P_1 - 1s^2\ ^1S_0$  intercombination-line transitions in heliumlike ions, Laughlin [17] concluded that “due to the breakdown of  $LS$  coupling, a first-order perturbation scheme employing nonrelativistic wave functions should not be employed to calculate intercombination-line transition rates for ions whose net positive charge is greater than 12.” Another point of view was expressed by Kim [18] who studied the strengths and weaknesses of relativistic atomic-structure calculations. Kim noted that “transition probabilities for a spin-forbidden transition, in a relativistic formulation is usually obtained as a result of cancellation that is very sensitive to the difference in the radial functions of the same  $l$  but different  $j$ 's, such as  $2p_{1/2}$  and  $2p_{3/2} \dots$ . In fact, a nonrelativistic calculation using a perturbation method would be more reliable because no such cancellation occurs in the nonrelativistic calculation.”

Relativistic mixing of  $LS$  states plays a crucial role in determining the radiative rates from the  $1s2p\ ^3P_1$  and  $1s3p\ ^3P_1$  levels. In pure  $LS$  coupling, the transition from a  $^3P$  level to the  $^1S$  ground state is forbidden. Therefore, the only way in which this radiation can be produced in the Breit-Pauli approximation is through the spin-orbit interaction that mixes the  $^1P_1$  and the  $^3P_1$  levels. The product of the square of the term-coupling coefficient [ $(0.036)^2 = 0.00131$ ] and the radiative rate for the transition  $1s2p\ ^1P_1 \rightarrow 1s^2\ ^1S_0$  ( $2.01 \times 10^{13}$  Hz) gives the calculated value of  $2.63 \times 10^{10}$  Hz for the  $1s2p\ ^3P_1 \rightarrow 1s^2\ ^1S_0$  transition. The spin-orbit interaction is calculated perturbatively in the Breit-Pauli approximation, whereas in the rela-

tivistic framework, it is introduced in the zeroth order through the use of the Dirac equation.

We investigated the importance of two effects on the non-relativistic orbitals that could, in turn, affect the radiative rates from the levels of the  $1s2p$  and  $1s3p$  configurations to the ground state. As mentioned previously, the  $1s$  orbital used in our excitation calculations was determined from a HF calculation on the  $1s^2$  ground state. However, the  $1s$  orbitals in the  $1snl$  configurations relax as compared to the  $1s$  orbital in  $1s^2$ . In a ten-times ionized species, one would expect this orbital relaxation to be small. Nevertheless, it was investigated because of the sensitivity of the  $1snp\ ^3P_1 \rightarrow 1s^2\ ^1S_0$  radiative rates to the amount of mixing between the  $^3P_1$  and the  $^1P_1$  levels. In order to include this effect, we first generated a new  $1s$  orbital from a single-configuration HF calculation on the  $1s2p\ ^3P$  term. We then corrected the  $1s$  orbital in the  $1s^2\ ^1S$  term by performing a multiconfiguration Hartree-Fock (MCHF) [19] calculation in which we minimized the energy of the  $1s^2\ ^1S$  term and included the  $1s^2\ ^1S$ ,  $1s2s\ ^1S$ ,  $1s3s\ ^1S$ ,  $1s4s\ ^1S$ , and  $1s5s\ ^1S$  terms, with all orbitals but the  $5s$  pseudo-orbital frozen.

The second effect we considered was the variation of orbitals with the  $LS$  term ( $LS$  term dependence). The largest effect of term dependence in He-like ions would be expected to occur in the  $1snp$  configurations where two different  $np$  orbitals should be used to describe  $^3P$  and  $^1P$  terms. This should be small in  $\text{Mg}^{10+}$ ; furthermore, it is already partially included in our previous structure calculations through configuration interaction between terms of the  $1snp$  configurations. Nevertheless, in order to more completely include this effect, we used the following procedure. The  $np$  orbitals with ( $n=2, 3$ , and  $4$ ) were first obtained from a series of  $1snp\ ^3P$  single-configuration Hartree-Fock calculations. Then, we introduced a  $5p$  pseudo-orbital to correct for term dependence in the  $2p$  orbital by performing a MCHF calculation that included the  $1s2p\ ^1P$ ,  $1s3p\ ^1P$ ,  $1s4p\ ^1P$ , and  $1s5p\ ^1P$  terms, and minimized the energy of the  $1s2p\ ^1P$  term by varying the  $5p$  orbital with all other orbitals frozen. Finally, we corrected the  $3p$  orbital for term dependence by generating a  $6p$  pseudo-orbital in a MCHF calculation in which we minimized the energy of the  $1s3p\ ^1P$  term and included the  $1s3p\ ^1P$ ,  $1s2p\ ^1P$ ,  $1s4p\ ^1P$ ,  $1s5p\ ^1P$ , and  $1s6p\ ^1P$  terms.

The dominant radiative transition rates to the ground level, determined by using the orbitals from these MCHF calculations in a Breit-Pauli configuration-interaction calculation, are also shown in Table I. The most sophisticated calculation performed to date for the  $1s2p-1s^2$  transitions is a relativistic many-body theory calculation by Johnson *et al.* [20], who obtained  $3.375 \times 10^{10}$  Hz for the intercombination transition and  $1.948 \times 10^{13}$  Hz for the resonant transition. As can be seen, our MCHF results show improved agreement with those of Johnson *et al.* [20] for the intercombination transition. This is primarily due to the inclusion of relaxation in the  $1s$  orbital, which slightly increases the mixing between the  $^3P_1$  and the  $^1P_1$  levels. The additional term-dependence included in the MCHF calculation was found to have little effect on this rate.

It should be pointed out that the electron-impact excitation from the ground state to the  $^3P_1$  levels is not as sensitive to the amount of  $^3P_1-^1P_1$  mixing, since this process is less selective and includes exchange and different partial waves. Therefore, orbital relaxation has very little effect on excitation to the  $^3P_1$  levels, and the CAHF orbitals should provide accurate cross sections for these transitions.

### III. COLLISIONAL-RADIATIVE AND EMISSIVITY CALCULATIONS

#### A. Isolated-ion approximation for Maxwellian plasmas

Our application of collisional-radiative theory to the calculation of level populations and emissivities for  $\text{Mg}^{10+}$  is based on the atomic data and analysis (ADAS) package [21]. ADAS is an interconnected set of computer codes and data collections developed at JET for modeling the radiating properties of ions and atoms in magnetic fusion plasmas and for assisting in the analysis and interpretation of spectral measurements.

The excitation cross sections were Maxwellian-averaged to obtain effective collision strengths over a range of electron temperatures from  $10^5$  to  $10^8$  K. These were used within ADAS to determine excitation and de-excitation rate coefficients. These rate coefficients, in combination with the radiative rates, were then employed to determine the level populations by solving the system of coupled equations given by

$$\frac{dN_j}{dt} = \sum_{i < j} N_i N_e Q_{ij} + \sum_{k > j} N_k (N_e Q_{kj} + A_{kj}) - N_j \left[ \sum_{i < j} (N_e Q_{ji} + A_{ji}) + \sum_{k > j} N_e Q_{jk} \right], \quad (1)$$

where a static approximation is assumed:

$$\frac{dN_j}{dt} = 0, \quad (2)$$

and where  $N_j$  is the population number density of level  $j$ ,  $N_e$  is the electron density,  $Q_{ij}$  is the electron-impact excitation rate coefficient for the  $i \rightarrow j$  transition, and  $A_{ji}$  is the spontaneous radiative rate for the  $j \rightarrow i$  transition. Once the level

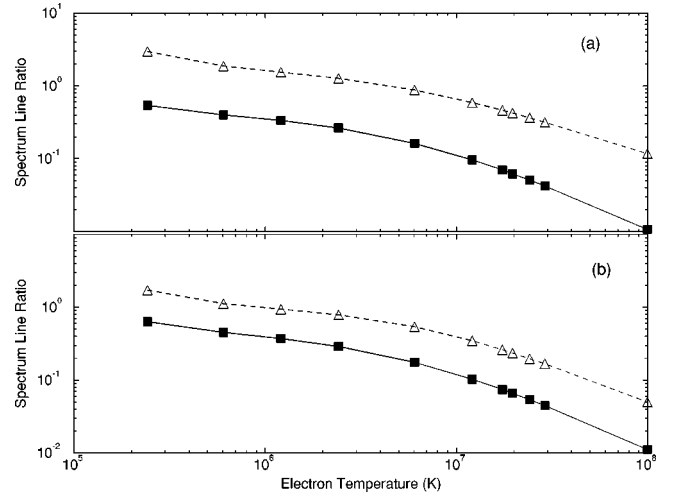


FIG. 5. Emission line ratio for the  $K\alpha_2/K\alpha_1$  transitions at (a)  $N_e = 10^8 \text{ cm}^{-3}$ , and (b) at  $N_e = 10^{12} \text{ cm}^{-3}$ . Solid curves are results that include all low-order electric and magnetic multipole radiative transitions between all 31  $LSJ$  levels included in the collisional-radiative model. Dashed curves are results in which only electric-dipole ( $E1$ ) radiative transition rates have been included.

populations have been determined for a given electron temperature and density, the  $i \rightarrow g$  over  $j \rightarrow g$  emission line ratio is given by

$$\frac{I_{i \rightarrow g}}{I_{j \rightarrow g}} = \frac{N_i A_{ig}}{N_j A_{jg}}. \quad (3)$$

We first assumed an isolated-ion approximation, where recombination, ionization, and charge-exchange contributions from adjacent ions, as well as emission from satellite transitions, were not included.

In this paper we focused on two line ratios involving soft-x-ray transitions. In Fig. 5 we show the  $K\alpha_2/K\alpha_1$  ( $1s2p \ ^3P_1 \rightarrow 1s^2 \ ^1S_0$  over  $1s2p \ ^1P_1 \rightarrow 1s^2 \ ^1S_0$ ) emission line ratio, using the 31-state  $R$ -matrix calculation. Results are shown for electron densities  $N_e = 10^8 \text{ cm}^{-3}$  (part a) and  $N_e = 10^{12} \text{ cm}^{-3}$  (part b). At the plasma conditions studied in the present paper, the populations of the excited levels are extremely small. We found that our modeling calculations were insensitive to whether we employed our 17-state ICFT  $R$ -matrix, 31-state ICFT  $R$ -matrix, or 31-level relativistic distorted-wave results, for the electron-impact excitation processes. Therefore, we make the following conclusions concerning the excitation cross-section calculations. First, the resonance structures in the excitation cross sections (not included in the distorted-wave calculation) produce a negligible effect on the population of the levels. Second, the presence of the  $1s4l$  levels (included in the 31-state calculation but not in the 17-state calculation) does not affect the population of the other levels. Thus, at the plasma conditions studied in this paper, the cascades are negligible. Third, relativistic effects on the excitation processes are sufficiently well determined by a semirelativistic approximation.

Since the population of the surrounding levels is extremely small, we can make an approximation that mimics

the full collisional-radiative model, neglecting any population mechanism other than excitations from the ground state. Using this approximation, the  $I_{i \rightarrow g}/I_{j \rightarrow g}$  line ratio, where  $i$  and  $j$  are the  $1s2p\ ^3P_1$  and  $1s2p\ ^1P_1$  levels, now becomes

$$\frac{I_{K\alpha_2}}{I_{K\alpha_1}} = \frac{I_{i \rightarrow g}}{I_{j \rightarrow g}} \approx \frac{Q_{gi}}{Q_{gj}} \frac{A_{ig}}{\sum_{k < i} A_{ik}} \frac{\sum_{k < j} A_{jk}}{A_{jg}} = \frac{Q_{gi} B_{ig}}{Q_{gj} B_{jg}}, \quad (4)$$

where  $B_{ig}$  is the radiative branching ratio for level  $i$ . For the  $K\alpha$  line ratio, both branching ratios are very close to one; therefore, it is not sensitive to the radiative rate from  $1s2p\ ^3P_1$  to  $1s^2\ ^1S_0$ , which depends on the very weak spin-orbit mixing between the  $^1P$  and  $^3P$  terms.

In the above line ratio calculations we include all the electric-dipole radiative transitions, calculated from our MCHF calculations; these were supplemented by magnetic-dipole and electric- and magnetic-quadrupole radiative transitions, calculated by using the HULLAC code. We have also included the two-photon radiative transition from the  $1s2s\ ^1S_0$  to the  $1s^2\ ^1S_0$  level. The rate of this transition, calculated by Derevianko and Johnson [22], is  $3.249 \times 10^{10}$  Hz. In order to test the importance of the higher-order multipoles, we carried out calculations of the line ratios when only electric-dipole transitions were included in the collisional-radiative equations. This would seem to be a good approximation, since the other radiative rates are small. However, as shown in Fig. 5 (dashed curves), neglecting the generally weaker electric-quadrupole, magnetic-dipole, and magnetic-quadrupole radiative rates produces more than an order of magnitude overestimation of the electron temperature. In particular, we found a fundamental role played by the radiative transition from the first excited level  $1s2s\ ^3S_1$  to the ground state. This transition is well known for its considerable astrophysical importance [23], and it is called the  $z$  transition in the spectroscopic notation of Gabriel [24]. The  $1s2s\ ^3S_1 \rightarrow 1s^2\ ^1S_0$  is a relativistic magnetic-dipole transition [25] (vanishes in the nonrelativistic limit), and our HULLAC calculation produced a rate of  $7.26 \times 10^4$  Hz, which compares very well with the value  $7.29 \times 10^4$  Hz calculated using relativistic many-body theory by Johnson *et al.* [26].

By neglecting this transition, the first excited level cannot radiate at all, and this has the following effect. First of all, collisional excitations from the ground state are now sufficient to significantly populate this level, even at low electron densities. Second, through direct excitation from  $1s2s\ ^3S_1$ , and by the multistep process consisting of excitation from  $1s2s\ ^3S_1$  to  $1s2p\ ^3P_2$ , followed by collisional de-excitation to  $1s2p\ ^3P_1$ , the population of the  $1s2p\ ^3P_1$  level is significantly enhanced. Therefore, the  $K\alpha$  line ratio increases when the magnetic-dipole transition rate from the  $1s2s\ ^3S_1$  to the ground state is not included in the calculation, as is shown in Fig. 5. At very low electron densities, we found that the  $K\alpha$  line ratio is also affected by whether the two-photon radiative transition  $1s2s\ ^1S_0 \rightarrow 1s^2\ ^1S_0$  is included or not. Neglecting this transition has the effect of increasing the population of the  $1s2s\ ^1S_0$  level substan-

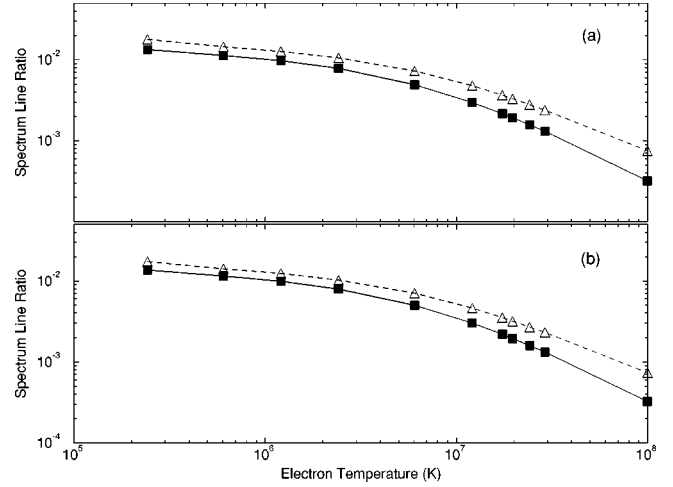


FIG. 6. Emission line ratio for the  $K\beta_2/K\beta_1$  transitions at (a)  $N_e = 10^8\ \text{cm}^{-3}$  and (b) at  $N_e = 10^{12}\ \text{cm}^{-3}$ . Solid curves are results that include all low-order electric and magnetic multipole radiative transitions between all 31  $LSJ$  levels included in the collisional-radiative model. Dashed curves are results in which only electric-dipole ( $E1$ ) radiative transition rates have been included.

tially, modifying the population of the surrounding levels. At low density, the  $1s2s\ ^1S_0$  level populates the  $1s2p\ ^3P_1$  level by radiative decay, producing an enhancement in the  $K\alpha$  line ratio. When the electron density increases, the main depopulation mechanism of the metastable  $1s2s\ ^1S_0$  level is the excitation to the  $1s2p\ ^1P_1$  level, and that produces a decrease in the  $K\alpha$  line ratio. This explains the differences between part (a) and (b) on Fig. 5. At low densities, neglecting both transitions from the  $1s2s$  levels to the ground state increases the  $K\alpha$  line ratio, while at higher densities, neglecting each one of these transitions has the opposite effect, producing a smaller overall effect.

One may wonder about the sensitivity of these calculated line ratios to the value of the magnetic-dipole and two-photon radiative rates. We found that when the first excited level is allowed to decay radiatively, the calculations are no longer sensitive to the magnitude of the decay rate. At low electronic densities, arbitrarily decreasing the magnetic-dipole radiative transition rate from  $1s2s\ ^3S_1$  to the ground state by a factor of  $10^3$  did not affect the  $K\alpha$  line ratio. For  $N_e = 10^{12}\ \text{cm}^{-3}$ , we found that decreasing the rate by a factor of 5 changed the  $K\alpha$  line ratio by only 10%. Furthermore, increasing the magnetic-dipole radiative rate had no effect on the ratio. We discovered the same insensitivity of the  $K\alpha$  line ratio to the magnitude of the two-photon rate. Decreasing it by a factor of  $10^3$  changed the ratio by only about 5%, while increasing the rate had no effect.

In Fig. 6 we show the  $K\beta_2/K\beta_1$  ( $1s3p\ ^3P_1 \rightarrow 1s^2\ ^1S_0$  over  $1s3p\ ^1P_1 \rightarrow 1s^2\ ^1S_0$ ) emission line ratio, determined using the full 31-level model. The same arguments are valid here, with respect to the radiative transitions included in the collisional-radiative model. For this line ratio, it was also important to include the relativistic magnetic-dipole transition from the  $1s2s\ ^3S_1$  level to the ground state. Otherwise, the population of the  $1s3p\ ^3P_1$  level would be overestimated. In contrast to the  $1s2p$  levels, the  $1s3p$  levels are

TABLE II.  $K\alpha$  line ratio for  $\text{Mg}^{10+}$  at an energy of 1500 eV.

$N_e$	Maxwellian energy distribution	Electron-beam energy distribution
$10^8 \text{ cm}^{-3}$	0.07	0.25
$10^{12} \text{ cm}^{-3}$	0.08	0.26

more likely to radiate to lower levels other than the ground state, and the radiative branching ratios [Eq. (4)] are different. Therefore, the  $K\beta$  line ratio is not independent of the radiative transition from  $1s3p \ ^3P_1$  to  $1s^2 \ ^1S_0$ . As the results show, both line ratios provide a very useful electron temperature diagnostic since they are insensitive to changes in the electron density.

### B. Isolated-ion approximation for electron-beam plasmas

In support of current spectral measurements of highly-charged heliumlike ions using an electron-beam ion trap [26], we carried out additional collisional-radiative calculations in which the Maxwellian energy distribution was replaced by a monoenergetic-beam energy distribution. The line ratios involving the  $1s2p$  levels at 1500 eV are presented in Table II for both a Maxwellian and an electron-beam plasma, while the line ratios involving the  $1s3p$  levels at 1700 eV are presented in Table III. The non-Maxwellian beam line ratios are larger than the Maxwellian line ratios in both cases, since the energies were chosen to be just above the excitation thresholds. As one would expect, the collisional excitation cross sections for the spin-changing transitions from  $1s^2 \ ^1S_0$  to  $1snp \ ^3P_1$  have a much different energy dependence than the excitation cross sections for the dipole-allowed transition from  $1s^2 \ ^1S_0$  to  $1snp \ ^1P_1$  (see Figs. 3 and 4). When the rate coefficient is determined using a Maxwellian distribution it is affected by the drop in the  $^3P_1$  cross sections at high energies. Consequently, the line ratios decrease when compared to the non-Maxwellian beam line ratios.

### C. Ionization, recombination, and satellite transitions

In an attempt to find other possible mechanisms that affect the intensity ratios, we calculated the contribution from radiative and dielectronic recombination (DR) of hydrogenic  $\text{Mg}^{11+}$ . Using a distorted-wave approximation implemented in the AUTOSTRUCTURE code [27,28], detailed calculations of the radiative recombination from the  $\text{Mg}^{11+}$   $1s$  ground state to all the 31 levels of the  $\text{Mg}^{10+}$  ion were performed. We also made detailed distorted-wave calculations of the DR rate coefficient from the  $1s$  level. We included in our calcu-

 TABLE III.  $K\beta$  line ratio for  $\text{Mg}^{10+}$  at an energy of 1700 eV.

$N_e$	Maxwellian energy distribution	Electron-beam energy distribution
$10^8 \text{ cm}^{-3}$	$1.9 \times 10^{-3}$	$8.9 \times 10^{-3}$
$10^{12} \text{ cm}^{-3}$	$2.0 \times 10^{-3}$	$9.0 \times 10^{-3}$

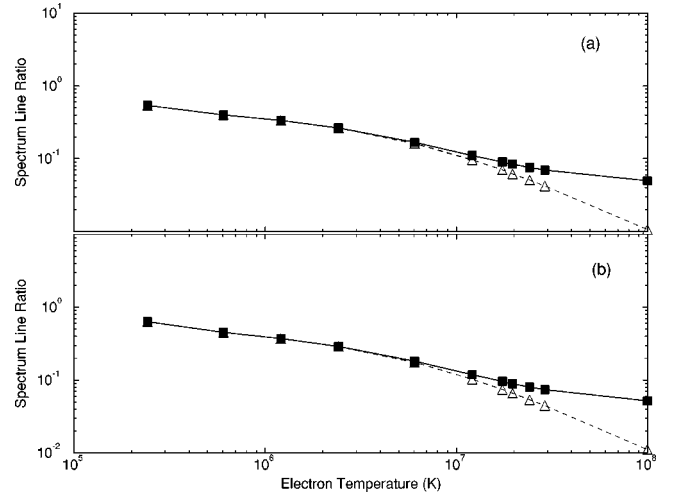


FIG. 7. Emission line ratio for the  $K\alpha_2/K\alpha_1$  transitions at (a)  $N_e = 10^8 \text{ cm}^{-3}$  and (b) at  $N_e = 10^{12} \text{ cm}^{-3}$ . Solid curves are results that include ionization to, and radiative and dielectronic recombination from, the  $1s$  ground-state level of the hydrogenic  $\text{Mg}^{11+}$  ion. Dashed curves are results that neglect this contribution.

lations all the intermediate  $2snl$  and  $2pnl$  ( $n=2,5$ ) autoionizing levels, and the cascade contributions from those high-lying levels. We found that the DR rate coefficients are not negligible, and for some particular levels DR is the main recombination mechanism. We also calculated direct ionization rate coefficients from every level to the  $\text{Mg}^{11+}$   $1s$  ground state, using the parametrized Lotz formula [29]. Charge-exchange contributions from adjacent ions were not included in this paper.

We modified the system of coupled equations [Eq. (1)] in order to calculate the contribution of recombination to the emission line ratios. The total recombination rate coefficients, together with ionization rate coefficients, were included in the system of rate equations that also included the  $1s$  level of  $\text{Mg}^{11+}$ . In Fig. 7 we show the  $K\alpha_2/K\alpha_1$  emission line ratio including the recombination contribution from the hydrogenic  $\text{Mg}^{11+}$  ion (solid lines), and neglecting this contribution (dashed lines). At low electron temperatures, the relative population of the hydrogenic ion is negligible, and therefore cannot contribute to the line emission of the He-like ion. At higher temperatures, recombination becomes very important, and enhances the intensity of the  $K\alpha_2$  over  $K\alpha_1$ . Figure 8 shows the  $K\beta_2/K\beta_1$  emission line ratio including the recombination contribution from the hydrogenic ion (solid lines), and neglecting this contribution (dashed lines). The same argument about the behavior of the line ratios as a function of the electron temperature is valid here. We found that the contribution of ionization from the excited levels is negligible for this plasma regime.

An additional mechanism that can affect the measurement of the line ratios is the presence of emission lines from lithiumlike  $\text{Mg}^{9+}$  which overlap with the heliumlike resonance lines. In particular, lithiumlike satellite transitions of the type  $1s2lnl' \rightarrow 1s^2nl$  and  $1s3lnl' \rightarrow 1s^2nl$  need to be taken into account. These satellite transitions broaden the heliumlike emission feature and could result in an overestimate of the

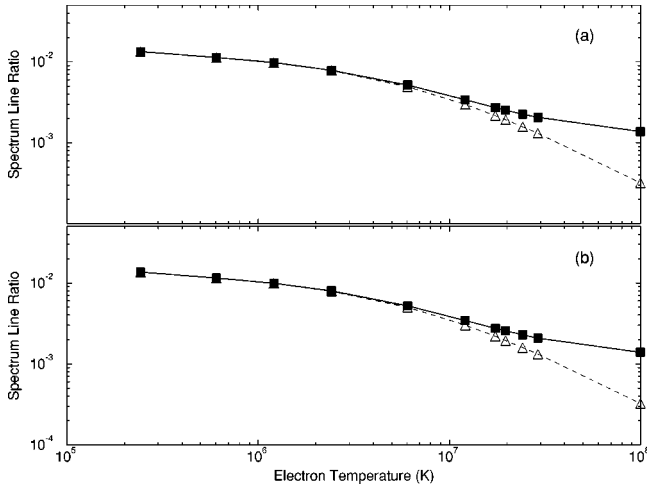


FIG. 8. Emission line ratio for the  $K\beta_2/K\beta_1$  transitions at (a)  $N_e = 10^8 \text{ cm}^{-3}$  and (b) at  $N_e = 10^{12} \text{ cm}^{-3}$ . Solid curves are results that include ionization to, and radiative and dielectronic recombination from, the  $1s$  ground-state level of the hydrogenic  $\text{Mg}^{11+}$  ion. Dashed curves are results that neglect this contribution.

density if ignored in modeling calculations. Experimental and theoretical investigations show that, in dense and cold Mg plasmas, the satellite structures of resonance lines can become more intense than the resonance lines themselves. The dominant role of  $K\alpha$  dielectronic satellites in the radiation spectra of Mg laser produced plasmas has been demonstrated by Rosmej *et al.* [30,31]. At electronic densities higher than  $10^{21} \text{ cm}^{-3}$ , and at a low electron temperature ( $\approx 80 \text{ eV}$ ), the  $1s2nl'$  manifold becomes at least as intense as the  $K\alpha_1$  resonance line and many intense satellites overlap the  $K\alpha_2$  intercombination line, resulting in a broad asymmetric spectral feature. The lines of high-intensity  $K\beta$  dielectronic satellites  $1s3lnl'$  in dense laser-produced Mg plasmas have also been investigated by Rosmej *et al.* [32]. The  $1s3l3l'$  satellites are found on the long-wavelength side of the  $K\beta_2$  line, the  $1s3l4l'$  satellites overlap with the  $K\beta_2$  intercombination line, and the high- $n$  satellites blend with the  $K\beta_1$  resonance line. Because  $K\beta_2$  is a weak feature, any enhancement from blends with dielectronic satellites could be substantial and make a large difference in the  $K\beta$  line ratios.

We performed detailed calculations of the lithiumlike satellite spectra, including all levels in the  $1s^2nl$ ,  $1s2snl$ ,  $1s2pnl$ ,  $1s3snl$  and  $1s3pnl$  ( $n=2,5$ ) configurations, assuming that these levels are populated by dielectronic capture from the  $1s^2$ ,  $1s2s$ , and  $1s2p$  levels of the He-like ions. The capture rates from the excited heliumlike levels are huge compared to the capture from the ground state, due to the different energies and autoionization rates. Under typical conditions of laser-produced plasmas near the target surface (cold dense and optically thick plasmas), this is the main mechanism that produces the strong satellite lines. However, we found that at low densities, the population of the excited  $1s2l$  heliumlike levels are negligible, and therefore the intensity from dielectronic satellites  $1s3lnl'$  is negligible.

It is important to emphasize that both the recombination contribution and the dielectronic satellites can be eliminated

in an electron-beam experiment. The recombination contribution can be eliminated if the energy of the electrons is smaller than the first ionization limit. Since the dielectronic recombination is a resonant process, a narrow electron-beam excitation can produce the heliumlike line, separately from the dielectronic satellites, which allows one to separate the relative contributions to the weak intercombination-line feature.

#### IV. SUMMARY

Using  $R$ -matrix theory, electron-impact excitation cross sections and rate coefficients were determined for  $\text{Mg}^{10+}$ . An intermediate-coupling frame transformation of the  $LS$ -coupled unphysical  $K$  matrices allowed cross sections to be obtained for all 465 transitions among the 31  $LSJ$  levels of the  $1s^2$ ,  $1s2l$ ,  $1s3l$ , and  $1s4l$  configurations. An independent check on the excitation cross sections was made using relativistic distorted-wave theory. Pseudo-orbitals determined from MCHF calculations were used to correct for orbital relaxation and term dependence in a Breit-Pauli calculation of the electric-dipole radiative transitions. A fully relativistic theory was used for all the other low-order electric and magnetic multipole transitions. These calculations were made to complete the construction of a collisional-radiative atomic data set for  $\text{Mg}^{10+}$ , which is now available at the ORNL Controlled Fusion Atomic Data Center (internet site: <http://www.cfadc.ornl.gov>).

The ADAS collisional-radiative modeling codes and the  $\text{Mg}^{10+}$  atomic data set were used to calculate equilibrium populations for all 31  $LSJ$  levels over a range of electron temperatures and densities. Spectral intensities for the  $1snp \ ^3P_1 \rightarrow 1s^2 \ ^1S_0$  and  $1snp \ ^1P_1 \rightarrow 1s^2 \ ^1S_0$  transitions were then calculated to produce  $K\alpha$  and  $K\beta$  line ratios. Neither line ratio is sensitive to the effects of resonances in the excitation cross sections, included in the  $R$ -matrix calculations and neglected in the relativistic distorted-wave calculations. Also, the effect of cascades is negligible.

The intercombination radiative rates depend on very weak spin-orbit mixing between the  $^1P$  and  $^3P$  terms, and comparison with sophisticated relativistic many-body perturbation theory calculations indicate that orbital-relaxation effects are important in the determination of reasonably accurate radiative rates for these transitions. The  $K\alpha$  line ratio is not sensitive to the intercombination radiative rate; however, the  $K\beta$  line ratio has a linear dependence on this radiative rate, and this is the largest source of uncertainty in this ratio.

These results show the importance of including the relativistic magnetic-dipole radiative transition  $1s2s \ ^3S_1 \rightarrow 1s^2 \ ^1S_0$  in the calculations, otherwise, the excited level  $1s2s \ ^3S_1$  cannot radiate at all, resulting in an overestimation of the line ratios. At very low electron densities, the two-photon radiative transition  $1s2s \ ^1S_0 \rightarrow 1s^2 \ ^1S_0$  has to be included in the calculations, since it affects the  $K\alpha$  line ratio.

Radiative and dielectronic recombination of hydrogenic  $\text{Mg}^{11+}$  produces an enhancement of both  $K\alpha$  and  $K\beta$  line ratios, at temperatures higher than 800 eV where the hydrogenic population becomes dominant. The detailed recombina-

nation rate coefficients, needed for the collisional-radiative atomic data set for  $\text{Mg}^{10+}$ , are also provided at the ORNL web site. We found that the dielectronic satellites lines, even though they overlap with the heliumlike lines, have a negligible intensity at the conditions studied in this paper. Since both line ratios have a weak dependence on the electron density, they provide useful electron temperature diagnostics for low-density plasmas.

## ACKNOWLEDGMENTS

We would like to thank Dr. Nigel Badnell and Dr. Peter Beiersdorfer for several useful discussions. This work was supported in part by the U.S. Department of Energy. Some of the computational work was carried out at the National Energy Research Supercomputer Center at Lawrence Berkeley National Laboratory.

- 
- [1] P. G. Burke and K. A. Berrington, in *Atomic and Molecular Processes: an R-matrix Approach* (IOP Press, Bristol, 1993).
- [2] A. Bar-Shalom, M. Klapisch, and J. Oreg, *Phys. Rev. A* **38**, 1773 (1988).
- [3] S. S. Tayal, *Phys. Rev. A* **35**, 2073 (1987).
- [4] D. C. Griffin, N. R. Badnell, and M. S. Pindzola, *J. Phys. B* **31**, 3713 (1998).
- [5] H. P. Summers and M. B. Hooper, *Plasma Phys.* **25**, 1311 (1983).
- [6] E. Källne, in *Physics of Highly-Ionized Atoms*, NATO Advanced Study Institute, Series B: Physics, Vol. 201, edited by R. Marrus (Plenum, New York, 1989), p. 245.
- [7] N. C. Woolsey, B. A. Hammel, C. J. Keane, A. Asfaw, C. A. Back, J. C. Moreno, J. K. Nash, A. Calisti, C. Mosse, R. Stamm, B. Talin, L. Klein, and R. W. Lee, *Phys. Rev. E* **56**, 2314 (1997).
- [8] P. Beiersdorfer, A. L. Osterheld, T. W. Phillips, M. Bitter, K. W. Hill, and S. von Goeler, *Phys. Rev. E* **52**, 1980 (1995).
- [9] F. B. Rosmej, *Phys. Rev. E* **58**, R32 (1998).
- [10] G. V. Brown, P. Beiersdorfer, D. A. Liedahl, K. Widmann, and S. M. Kahn, *Astrophys. J.* **502**, 1015 (1998).
- [11] A. J. Smith, P. Beiersdorfer, K. J. Reed, A. L. Osterheld, V. Decaux, K. Widmann, and M. H. Chen, *Phys. Rev. A* **62**, 012 704 (2000).
- [12] K. A. Berrington, W. B. Eissner, and P. H. Norrington, *Comput. Phys. Commun.* **92**, 290 (1995).
- [13] C. Froese-Fischer, *Comput. Phys. Commun.* **43**, 355 (1987).
- [14] A. Burgess, *J. Phys. B* **7**, L364 (1974).
- [15] J. Oreg, W. H. Goldstein, M. Klapisch, and A. Bar-Shalom, *Phys. Rev. A* **44**, 1750 (1991).
- [16] M. Klapisch, J. L. Schwob, B. S. Fraenkel, and J. Oreg, *J. Opt. Soc. Am.* **67**, 148 (1977).
- [17] C. Laughlin, *J. Phys. B* **11**, L391 (1978).
- [18] Y. K. Kim, *Phys. Scr.* **T73**, 19 (1997).
- [19] C. Froese-Fischer, *Comput. Phys. Commun.* **64**, 369 (1991).
- [20] W. R. Johnson, D. R. Plante, and J. Sapirstein, *Adv. At. Mol. Phys.* **35**, 255 (1995).
- [21] H. P. Summers, *ADAS User Manual* (JET-IR, Abingdom, UK, 1994).
- [22] A. Derevianko and W. R. Johnson, *Phys. Rev. A* **56**, 1288 (1997).
- [23] A. H. Gabriel and C. Jordan, *Phys. Lett. A* **32**, 166 (1970).
- [24] A. H. Gabriel, *Mon. Not. R. Astron. Soc.* **160**, 99 (1972).
- [25] G. W. Drake, in *Physics of Highly-Ionized Atoms*, NATO Advanced Study Institute, Series B: Physics, Vol. 201, edited by R. Marrus (Plenum, New York, 1989), p. 148.
- [26] P. Beiersdorfer (private communication).
- [27] N. R. Badnell, *J. Phys. B* **19**, 3827 (1986).
- [28] N. R. Badnell and M. S. Pindzola, *Phys. Rev. A* **39**, 1685 (1989).
- [29] W. Lotz, *Z. Phys.* **220**, 466 (1969).
- [30] F. B. Rosmej, A. Y. Faenov, T. A. Pikuz, Y. Skobelev, A. E. Stepanov, A. N. Starostin, V. S. Rerikh, V. A. Makhrov, F. Flora, S. Bollanti, P. Di Lazzaro, T. Letardi, K. Vigli-Papadaki, A. Nottola, A. Grilli, L. Palladino, A. Reale, A. Scafati, and L. Reale, *Pis'ma Zh. Éksp. Teor. Fiz.* **65**, 679 (1997) [*JETP Lett.* **65**, 708 (1997)].
- [31] F. B. Rosmej, A. Y. Faenov, T. A. Pikuz, F. Flora, P. Di Lazzaro, S. Bollanti, N. Lisi, T. Letardi, A. Reale, L. Palladino, D. Batani, S. Bossi, A. Bornardinello, A. Scafati, L. Reale, A. Zigler, M. Fraenkel, and R. D. Cowan, *J. Quant. Spectrosc. Radiat. Transf.* **58**, 859 (1997).
- [32] F. B. Rosmej, A. Y. Faenov, T. A. Pikuz, F. Flora, P. Di Lazzaro, T. Letardi, A. Grilli, A. Reale, L. Palladino, G. Tomassetti, A. Scafati, and L. Reale, *J. Phys. B* **31**, L921 (1998).